

A High Resolution Dilatometer Using Optical Fiber Interferometer

Xin Qin,^{1,2} Guoxin Cao,^{3,4} Mengqiao Geng,^{1,2} Shengchun Liu,^{3,4} and Yang Liu^{1,2}

¹*International Center for Quantum Materials, Peking University, Haidian, Beijing 100871, China*

²*Hefei National Laboratory, Hefei 230088, China*

³*College of Underwater Acoustic Engineering, Harbin Engineering University, Harbin 150001, China*

⁴*Acoustic Science and Technology Laboratory, Harbin Engineering University, Harbin 150001, China*

(*Electronic mail: liuyang02@pku.edu.cn)

(Dated: 14 May 2024)

We introduce a high performance differential dilatometer based on an all-fiber Michelson interferometer at cryogenic temperature with 10^{-10} resolution in $\delta L/L$. It resolve the linear thermal expansion coefficient by measuring the oscillating changes of sample thickness and sample temperature with the interferometer and in-situ thermometer, respectively. By measuring the linear thermal expansion coefficient α near the antiferromagnetic transition region of BaFe_2As_2 as a demonstration, we show our dilatometer is able to measure thin samples with sub-pm-level length change resolution and mK-level temperature resolution. Despite there is residual background thermal expansion of a few nm/K in measurement result, our new dilatometer is still a powerful tool for study of phase transition in condensed matter physics, especially has significant advantages in fragile materials with sub- $100\mu\text{m}$ thickness and being integrated with multiple synchronous measurements and tuning thanks to the extremely high resolution and contactless nature. The prototype design of this setup can be further improved in many aspects for specific applications.

I. INTRODUCTION

Thermal expansion coefficient α , the thermodynamical parameter that describes the relation between sample size (or volume) and temperature, carries crucial information about materials. Studying α across phase transition is of particular interest in condensed matter physics, since it is coupled to all phase transitions allowed by symmetry and can be linked to other parameters such as the specific heat C_V through the Ehrenfest and Maxwell relations¹. The thermal expansion measurement can detect phase transitions and dynamics properties of superconductors²⁻⁶, magnetic materials⁷⁻¹⁰ and even metallic glass and so on, which shows its unique advantages compared to resistivity and magnetic-susceptibility measurements.

Dilatometers measure the sample length $L(T)$ as a function of temperature T , the variation $\Delta L = L(T) - L(T_0)$ from its value at a reference temperature $T = T_0$, and then deduce the thermal expansion coefficient $\alpha = L^{-1}dL/dT$. Different approaches of measuring ΔL have been reported, using fiber Bragg grating^{11,12}, atomic microscope piezo-cantilever¹³, piezobender¹⁴, strain gauge technique^{15,16}, X-ray diffractions¹⁷, etc. The capacitive dilatometry, which measures ΔL through monitoring the capacitance between the sample surface and a metal reference surface, is one of the most widely used because of its supreme accuracy¹⁸⁻²². Its pm-resolution of ΔL corresponds to $\Delta L/L \sim 10^{-10}$ for samples with a length $L \leq 5$ mm, orders of magnitudes better than other methods.

Here we present a new approach which measures the samples' length variation contactlessly with a sensitivity of a few 10^{-10} in $\delta L/L$ for sub-milimeter-thickness sample using a high resolution optical fiber Michelson interferometer. We use a "true" differential method where the applied quasi-DC

sinusoidal temperature oscillation δT at f_S near T_0 induces an oscillation δL in L . So δL naturally has in-phase and out-of-phase components refer to δT , which are from the thermal transport delay because of sample thermal properties. When the sample is at equilibrium and has a uniform phase under AC temperature oscillation δT , there is no phase shift between δL and δT and the out-of-phase component is zero. The amplitudes of δL and δT , $\langle \delta L \rangle$ and $\langle \delta T \rangle$, can be measured using lock-in technique to deduce the linear thermal expansion coefficient $\alpha = L^{-1} \langle \delta L \rangle / \langle \delta T \rangle$. This setup can achieve extraordinary 0.5 pm resolution in $\langle \delta L \rangle$, 5×10^{-10} in $\delta L/L$ for 1-milimeter-thickness sample, and mK-level resolution in $\langle \delta T \rangle$, simultaneously. Thanks to the contactless nature of our optical approach, we can study fragile and thin samples, implement other synchronous measurements such as transport, as well as apply in-situ controls such as strain and electric field. In this work we demonstrate our dilatometer at liquid nitrogen temperatures while it can, in principle, be extended to temperatures ranging from sub-10 K up to room temperature.

This article is organized in the following order. We first describe the principle and design of our dilatometer and the extension for ultra-low temperature in Section II. We then calibrate its resolution, stability and precision in Section III. In Section IV, we apply this setup to study the phase transition of a thin BaFe_2As_2 crystal as a demonstration.

II. SETUP AND PRINCIPLE

A. Dilatometer Structure

Fig. 1 shows the structure of our dilatometer. In general, we design a setup which contains a fiber Michelson interferometer to measure δL and in-situ heater and thermometer to

apply and measure δT of sample. As shown in Fig. 1(a), the device is attached to the cold finger inside the cryostats through the upper screw thread (label 1). The beam splitter of the Michelson interferometer, i.e. the 50/50 fiber coupler (see next section), is installed inside the notch of fiber coupler holder (3), and its two 1-meter-length interference arms are wound on the two PZT rings (5). The whole structure is stacked on the PZT holders (4) and tightly fixed by the lock nut (2). The dimming frame (7) is mounted to the cold finger (1), inside which the grin-lens (11) is installed coaxially using the lens locker (12 and 13), see the enlarged plot in Fig. 1 (b). The sapphire sample holder (15) is mounted to an adjustable plate (10) positioned using three Ti fine adjusting screws (6) and springs (8). The coaxial and miniaturized design ensures the temperature uniformity within the structure and minimizes (internal) vibration. Its 30-mm-diameter and 70-mm-height size fit to most cryostats.

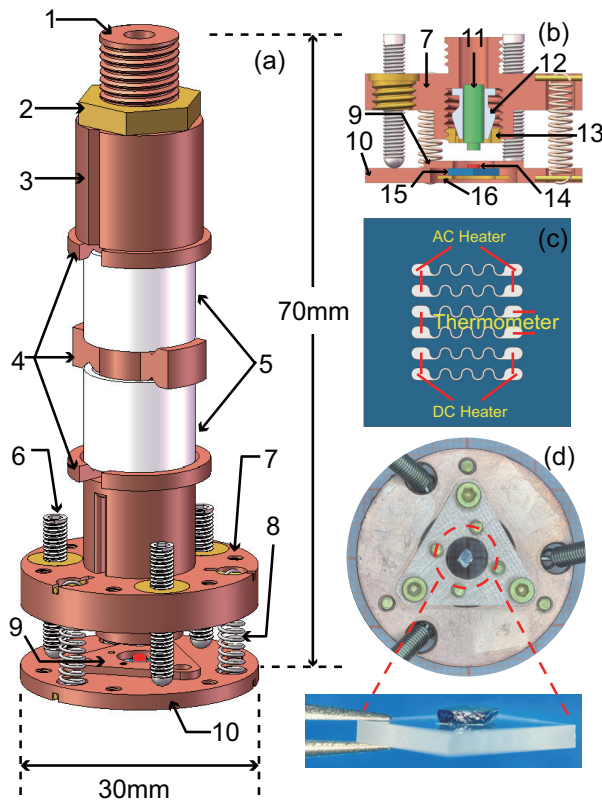


FIG. 1. Schematic drawing and photos of our dilatometer. (a) shows the entire structure, (b) shows a zoom-in cut-away view of the optical adjusting structure and sample-holding structure, (c) shows the design of in-situ thermometer, AC and DC heaters on the sapphire sample holder using six evaporated Pt wires. (d) shows a top-view photo of sample-holding structure with a sample (14) installed on the upper surface of sapphire sample holder (15) by extremely thin N-Grease, about $5 \mu\text{m}$ as measured, as shown in the zoom-in photo of sample installation. (1) cold finger, (2) lock nut, (3) fiber coupler holder, (4) PZT rings holders, (5) PZT rings, (6) Ti fine adjusting screws, (7) Dimming frame, (8) Be-Cu springs, (9) upper plate, (10) adjusted plate, (11) grin-lens, (12) and (13) lens locker, (14) sample, (15) sapphire sample holder, (16) Be-Cu lower plate. The structure component is made of oxygen-free-copper if not specifically stated.

We carefully arrange the upper and lower plates (9 & 15) and the sapphire sample holder (15), so that the lower surface of the sample (14) is perfectly aligned with the upper-surface of the adjustable plate, which is exactly the plane defined by the pivot of the three Ti fine adjusting screws (6). With this coplane design, we get rid of the background length change component from thermal expansion of sample-holding structure (9), (10), (15), (16) so that the background AC length change at measurement frequency f_S of entire system, δL_B , is limited to the distance change along the Z direction between the end of grin lens (11) and the pivot of three Ti fine adjusting screws (6), which is from the AC thermal expansion of 10-mm-long Ti fine adjusting screws (6), grin lens (11) and lens-holding structure (7), (12), (13).

Then we thermally isolate structures from sample by introducing δT only at sample and making sure it doesn't leak to fine adjusting screws (6) as well as other structures for further suppressing this background AC length change so that the length change measured by the interferometer origins only from the sample's thermal expansion. Firstly, we cool the entire structure to a low temperature and stabilize it with a system PID temperature controller using the cryostat thermometer and heater mounted on the cold finger. Then we introduce δT at sample directly by installing sample on the sapphire sample holder (15), which has six Pt wires evaporated on its lower surface as in-situ heaters and thermometer, as shown in Fig. 1(c). Two pairs of Pt wires are used as DC and AC heaters that the voltage V_{DCH} applied to the DC heater heats the sample temperature to T_0 , and an oscillating voltage V_{ACH} at f_S applied to the AC heater induces an oscillation δT to the sample DC temperature T_0 . δT leaks to Ti fine adjusting screws (6) through (9), (10) and three contact points between (6) and (10) and the thermal resistance and thermal capacity are large enough to reduce the δT at (7) is zero at a normally used AC heating frequency f_S , i.e. $f_S > 0.01\text{Hz}$, so the background AC length change at f_S is limited to the thermal expansion of 10-mm-long Ti fine adjusting screws (6) and our in-situ AC heating can also reduce the δT heating of fine adjusting screws (6) comparing with AC heating the entire structure. The central pair of Pt wires are calibrated by the cryostat thermometer and used to monitor the real-time sample temperature $T_0 + \delta T$ via lock-in technique. What's more, we introduce thermal insulation between the sample holder (15) and the upper and lower plate (9 & 16), as well as between the fine adjusting screws (6) and the adjusted plate (10). Besides, the adjusted plate (10) is relatively large and thermally shunted to the thermostatical cold finger (1) and the thermal expansion coefficient of Ti is very small. So the AC length fluctuation of the fine adjusting screws (6) is well reduced with the designs mentioned above.

We can model the temperature variation of the fine adjust screws (6) and minimize it further by carefully choosing the material/size of each part and changing the thermal link between different parts. Eventually, the thermal expansion of the fine adjust screws (6) becomes negligible for $f_S \gtrsim 0.1 \text{ Hz}$ even if the sample thickness is less than $100 \mu\text{m}$. The thermal equilibrium time of the sapphire sample holder (15) with thickness h is proportional to h^2 , and deformation caused by

thermal gradient is inversely proportional to h^3 . Our numerical modeling shows that if $h = 800 \mu\text{m}$, the temperature oscillation amplitude at the sapphire plate's upper surface is about half of the value at its lower surface when the AC heating frequency is set to about 10 Hz. Giving consideration to other effects such as the thermal resistance of the sample and between the sample and sapphire plate, we choose AC temperature oscillation frequency $f_S \lesssim 2 \text{ Hz}$ to measure α .

The in-situ heating is directly applied to the sample holder, so that the temperature of the rest parts of the dilatometer is stabilized within mK-level by the system PID temperature controller. Along with the excellent thermal uniformity among the entire structure and the minimal mismatch between the interferometer's two fiber arms, the thermal drift of this interferometer is much smaller and we get better measurement stability comparing with heating the entire structure.

B. Fiber Interferometer

As described in the previous section, we coat the upper surface of the sapphire sample holder (15) with an extremely thin layer of N-Grease (typically a few μm as we measured), and then gently press the sample (14) onto the surface, as the zoom-in photo of sample installation showed in Fig. 1(d). With the AC heater, we can impose a small temperature oscillation δT at frequency f_S onto a steady state temperature bias T_0 set by the DC heater. The real-time sample temperature $T_0 + \delta T$ can be measured by the thermometer on the lower surface of sapphire sample holder (15). We then use a fiber Michelson interferometer to measure the δT induced sample's thermal expansion δL . Because of the finite specific heat C and thermal conductivity κ of the sample and sample holder, there is always a delay $\tau \propto C/\kappa$ between sample temperature and the temperature read from in-situ thermometer. Since the thermal conduction of the thin grease and sapphire sample holder (15) is large, τ is usually limited by the sample, especially near phase transition region. Therefore, the measured δL naturally has in-phase and out-of-phase components refer to measured δT and the out-of-phase component has great potential for the simultaneous measurement of specific heat and thermal conductivity of sample around phase transitions²³. Typically the out-of-phase component is non-negligible when $f_S > 1 \text{ Hz}$. If we choose a small f_S so that $f_S \cdot \tau \ll 1$, we can neglect the out-of-phase component and measure the oscillation amplitude of δT and δL , $\langle \delta T \rangle$ and $\langle \delta L \rangle$, by digital lock-in technique to deduce the sample's thermal expansion coefficient at T_0 by:

$$\alpha_{T_0} = L^{-1} \frac{\langle \delta L \rangle}{\langle \delta T \rangle} \quad (1)$$

Then we sweep V_{DCH} applied to the DC heater to slowly tune DC temperature T_0 to sweep the α vs. T_0 continuously.

The measurement principle of our all-fiber Michelson interferometer is shown in Fig. 2. The 10 kHz-linewidth, $\lambda = 1550 \text{ nm}$ laser is equally distributed into the measurement and reference arms by a 2x2 fiber coupler. We use a grin-lens at the

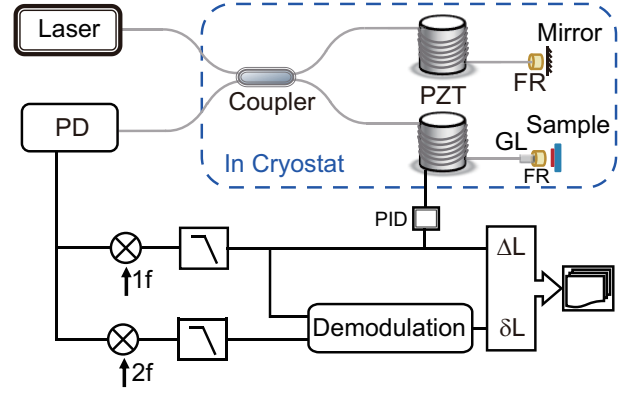


FIG. 2. Principle of our optical interferometer measurement. The AC & DC change of sample thickness, δL & ΔL , is translated to the change of AC and DC component of the total phase difference Φ , $\delta\phi_S$ & $\Delta\phi_S$, respectively. These changes can be deduced from the photo-detector's (PD's) output voltage. We wind the two arms or the fiber Michelson interferometer around two PZT rings tightly in order to apply phase modulation and feedback. We deduce the AC phase change δL from the demodulation output directly, and calculate the DC change of sample thickness ΔL from the feedback voltage.

end of the measurement arm to collimate the outgoing laser to be parallel and collect the light reflected from the upper surface of the sample, while the reference arm has an integrated mirror at its end. The diameter of laser spot on sample surface is about $450 \mu\text{m}$ and the light intensity we use is limited to be smaller than $100 \mu\text{W}$. With typical thermal anchoring, such a low light power can be used in cryogenic systems even down to sub-1 K temperatures without noticeable heating. The system signal to noise ratio (SNR) is influenced by the interference contrast of our interferometer, which is dependent on the ratio of collection light intensity of reflected light from sample surface and emission light intensity from grin lens. So for the best resolution we need the sample surface is flat on the scale of our laser spot size for better specular reflection of incidence parallel light, i.e. the cleavage surface of BaFe_2As_2 and the polished surface of Ag with a roughness of about $1.5 \mu\text{m}$ are enough for almost 100% specular reflection. Besides we should adjust three Ti fine adjusting screws (6) to make sure the reflected laser returns by the same route of emission laser and completely collected by the grin lens (11). The whole structure is coaxial and with 120° -rotational symmetry so the thermal expansion and vibration of structure don't affect the alignment we adjust initially in the atmosphere when we change the system temperature. The work distance of grin lens is $5 \sim 10 \text{ mm}$ so the influence of thermal expansion of structure over measurement temperature range, which is at level of μm , is negligible. Faraday-Rotation-Lenses (FR) are inserted before the sample/mirror in order to reduce the random polarization rotation of the wound fiber²⁴. The reflected laser beams interfere at the coupler so that the light intensity I at the output port is $I = I_0[1 + \cos(\Phi)]$, where I_0 is the interference intensity and Φ is the phase difference between these two fiber arms. The photodetector (PD) converts I into a voltage

signal.

We implement the PGC modulation/demodulation methods to improve the sensitivity in measuring Φ ²⁵. We tightly wind the reference arm around a PZT ring and apply an modulation voltage to introduce a phase modulation $\phi_M = C \cdot \cos(2\pi f_M t)$, where C is the modulation depth and f_M is the modulation frequency (\sim kHz). The modulated light intensity can be expanded according to the Jacobian angular expansion as:

$$\begin{aligned} I &= I_0[1 + \cos(C \cdot \cos(2\pi f_M t) + \Phi)] \\ &= I_0 \left\{ 1 + 2 \sin(\Phi) \sum_{N=0}^{\infty} J_{2N+1}(C) \cos[2\pi \cdot (2N+1) f_M t] \right. \\ &\quad \left. + \cos(\Phi) [J_0(C) + 2 \sum_{N=1}^{\infty} (-1)^N J_{2N}(C) \cos(2\pi \cdot 2N f_M t)] \right\} \end{aligned} \quad (2)$$

where J_N is the N-order Bessel function. We use lock-in technique to measure the amplitude V_1 and V_2 of the 1st and 2nd harmonic component of I at f_M and $2f_M$, and calculate Φ using the relation

$$\Phi = \frac{1}{2} \tan^{-1} \left(\frac{J_2(C)V_1}{J_2(C)V_2} \right) \quad (3)$$

Φ is the quasi-DC component of the total phase difference between the two arms. It consists a constant value due to the unequal optical length between the two arms and a oscillating signal from the sample's thickness oscillation $\delta\phi_S = 4\pi\delta L/\lambda$. It also has a slowly varying component $\Delta\phi$ caused by the thermal fluctuation of the fibers and PZTs, wavelength drifting of the laser, and the thermal expansion of the structure and sample ΔL induced by sweeping T_0 .

In order to compensate the slowly drifting $\Delta\phi$, we introduce a feedback phase by winding the measurement arm around another PZT ring and introduce a feedback voltage V_F to it. A simple feedback voltage can be achieved by filtering and amplifying the measured V_1 with an extremely long time constant (~ 300 s). Once the feedback gain G_F , which is now the ratio between the optical length change and V_1 , is large enough, The DC component of V_1 will be approximately zero. Since $\delta\phi_S$ is usually very small, V_1 is approximately proportional to $\delta\phi_S$ and V_2 is locked at the extremum $I_0 J_2(C)$. In short, by using this feedback, we simplify the measurement, improve the sensitivity of $\delta\phi_S$, and also solve the diverging problem caused by the \tan^{-1} function in equation (3). The AC length change δL can be then simply calculated from

$$\delta L = \frac{1550}{4\pi J_1(C) I_0} V_1 \quad nm \quad (4)$$

Meanwhile, the phase induced by the feedback voltage V_F compensates the quasi-DC change of the sample thickness and the thermal drifts from laser, fiber and structure. Therefore, if the drifts caused by the laser, fiber and PZT are small, and the thermal expansion of the structure ΔL_B is calibrated by a separate measurement, we can deduce the absolute change of the sample thickness ΔL from the feedback voltage V_F through

$$\Delta L = G_F V_F - \Delta L_B \quad (5)$$

We can also remove sample and evaporate 20-nanometer-thickness gold on the upper surface of sapphire sample holder (15) and it can reflect the incidence laser from grin lens (11) for background thermal expansion measurement. We can get the structure's DC thermal expansion is $\Delta L_B/\Delta T = G_F V_F/\Delta T \sim 20$ nm/K and its AC thermal expansion $\delta L_B/\delta T$ is about 4 nm/K at 130K. There is always a background AC thermal expansion $\delta L_B/\delta T$, about a few nm/K, among measurement temperature range and it is slightly different between different measurement cycles because of slightly different sample installation everytime so our prototype dilatometer can't measure the absolute value of α for now if the sample thermal expansion is as small as the background AC thermal expansion $\delta L_B/\delta T$. This background is smooth in temperature, and can be further reduced with better structural design. Fortunately, it does not affect its application in studying phase transitions, where the features in thermal expansion are rather sharp in temperatures. Therefore, our prototype fiber interferometer based dilatometer is a powerful tool in related studies, especially for its extremely high resolution and contactless nature.

Before ending this section, we would like to mention that our setup uses the combination of bend-resistant singlemode fiber and 45 degree faraday rotators at the end of each arm, in order to minimize the size²⁴. Alternatively, one can use polarization-maintaining fiber for the interferometer when measuring α in a magnetic field. At a cost, the diameter of the PZT rings should be more than 40 mm.

C. Extension for Ultra-low Temperature

Although as a prototype we only demonstrate our setup at liquid nitrogen temperature, this method can be extended to ultra-low temperatures.

The fiber and other optical components still work well in dilution refrigerator below 100 mK from our experience on another work of ultra-low temperature all-fiber MOKE measurement setup so the interferometer should function well. The piezoelectric coefficient of PZT rings decreases with system temperature cooling down and our experience is the piezoelectric coefficient at 1 K is about an order of magnitude smaller than which at room temperature. So feedback is not a problem because we need smaller feedback voltage V_F to cancel the DC drift ΔL because of the smaller thermal expansion coefficient in ultra-low temperature than room temperature. Besides, we can always identify the modulation depth C from V_1 , V_2 and I_0 so the variation of PZT performance doesn't affect the modulation and demodulation mentioned at II B. So the δL measurement is extensible for ultra-low temperature.

As for the δT and T_0 introducing and measurement, we can still use Pt wires for AC heating and DC heating. Other thermometers such as thermal couple should be used instead of the simple Pt wires. So this setup still works well at ultra-low temperature in principle.

III. RESOLUTION, STABILIZATION AND PRECISION

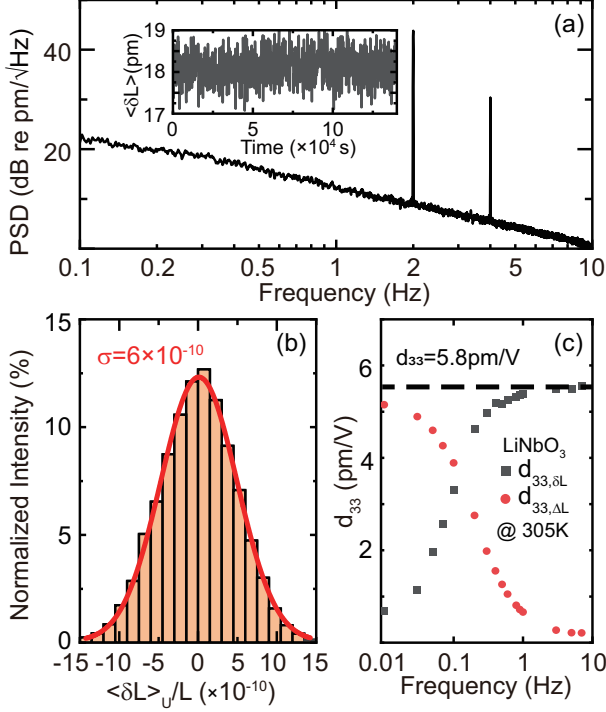


FIG. 3. Calibration of our optical interferometer measurement. (a) The Power Spectra Density (PSD) of δL . An AC sample thickness oscillation $\langle \delta L \rangle = 18$ pm is induced by $\langle \delta T \rangle = 1.5$ mK at $f_s = 2$ Hz for a 801-micrometer-thickness silver at $T_0 = 295$ K. The inset shows the AC oscillation amplitude $\langle \delta L \rangle$ with $t_c = 25$ s (black curve) and $t_c = 25$ s (red curve) for a 14000 s period. (b) Histograms of uncertainty of $\langle \delta L \rangle / L$, $\langle \delta L \rangle_U / L$, in inset of (a). The red line is a Gaussian fit with $\langle \delta L \rangle_U / L = 6 \times 10^{-10}$ standard deviation. (c) Measured piezoelectric coefficient d_{33} of 0.5 mm-thick Z-cut LiNbO₃ at 305 K. We apply an oscillating voltage of different frequencies on the sample's thickness-direction, measured its AC piezoelectric length change δL_D , and then calculate d_{33} using eq (9). $d_{33, \delta L}$ (black squares) is calculated from δL_D measured by δL and $d_{33, \Delta L}$ (red circles) is calculated using the δL_D measured from ΔL . The crossover between $d_{33, \Delta L}$ and $d_{33, \delta L}$ at about 0.1 Hz identifies the feedback bandwidth. The black dash line represent the expected d_{33} , i.e. $d_{33, \delta L}$ measured at sufficiently high frequency well above the feedback loop bandwidth. This figure can be used as a calibration of our interferometer if the absolute value of length oscillation is of interest.

For demonstrating the $\langle \delta L \rangle$ resolution of our dilatometer, we apply an AC temperature $\langle \delta L \rangle = 1.5$ mK at $f = 2$ Hz to a 801-micrometer-thickness silver to induce an extremely small δL about $\langle \delta L \rangle = 18$ pm at $T_0 = 295$ K. Fig. 3(a) shows the power spectrum density (PSD) of the raw δL signal measured by the interferometer, where the noise spectral density at frequency f_s is about $3.3 \cdot f_s^{-0.5}$ pm/√Hz. The two peaks corresponds to the first and second harmonic component of δL induced by an $f = 2$ Hz voltage applied to the AC heater and the noise spectral density at $f = 2$ Hz is about 8 dB re pm/√Hz,

as well as 2.5 pm/√Hz. The inset of Fig. 3(a) shows the measured $\langle \delta L \rangle$ by lock-in technology with $t_c = 25$ s in time domain, where t_c is the time constant of our lock-in algorithm, the same with time constant of commercial Lock-In Amplifier. The time constant t_c is a compromise between the measurement time and the resolution of $\delta L / L$. We can estimate the uncertainty of $\delta L / L$ is $\langle \delta L \rangle_U / L = \frac{2.5 \text{ pm} / \sqrt{\text{Hz}}}{\sqrt{t_c} \cdot L}$ at $f_s = 2$ Hz so $\langle \delta L \rangle_U / L$ is 6×10^{-10} for the $L = 801 \mu\text{m}$ silver when $t_c = 25$ s, as the histogram of data in inset of Fig. 3(a) showed in Fig. 3(b). It is improved by a factor of 2 for every 4-fold increase in t_c or f_s so it can reach remarkable 1×10^{-10} resolution if we choose $t_c = 900$ s. On the other hand, the change of T_0 during the averaging time t_c should be smaller than the $\langle \delta T \rangle$ so that the temperature resolution of our dilatometer is dependent on $\langle \delta T \rangle$. The $\langle \delta T \rangle$ can be as low as 5 mK in order to resolve the fine structures in α , e. g. the sharp α peak at the first order phase transition, see Fig. 4. So in typical measurement, the sweeping rate of T_0 , dT_0/dt , is usually about $0.1 \sim 1$ mK/s, and $\langle \delta T \rangle$ is about 0.5 K if there is no need for extremely high temperature resolution. Even under the worst of circumstances in which the sample is as thin as $L = 200 \mu\text{m}$ and we should measure at frequency as low as $f = 0.25$ Hz for thermal equilibrium of whole sample while AC heating, the resolution of α is still as low as $8 \times 10^{-9} \text{ K}^{-1}$ when $t_c = 25$ s, and 10^{-10} K^{-1} resolution is achievable by increasing t_c and $\langle \delta T \rangle$. For better measurement condition with thicker sample and higher measurement frequency f_s , the 10^{-10} K^{-1} resolution of α is easy to achieve.

In addition to its resolution, measuring α as accurate as possible is also of great interest. The precision in α is limited by the $\langle \delta L \rangle$ measurement, because the amplitude of the AC temperature oscillation, $\langle \delta T \rangle$, is proportional to the AC heating power V_{ACH}^2 and can be measured/calibrated with extremely high accuracy. We demonstrate the precision of $\langle \delta L \rangle$ by measuring the piezoelectric coefficient d_{33} of a Z-cut LiNbO₃ single crystal with thickness $L = 0.5$ mm. The upper and lower surfaces of sample are coated with 20 nm-thick Au film for gating. An AC voltage V_D is applied between these two gates to generate a thickness change δL_D , which is then measured by the interferometer as described in previous sections. The d_{33} is then deduced by:

$$d_{33} = \frac{\delta L_D / L}{V_D / L} = \frac{\delta L_D}{V_D} \quad (6)$$

Fig. 3(d) shows the measured d_{33} of LiNbO₃ at 305K. As described in last section, the sample's thickness change can either be deduced from the interferometer output, δL , or from the feedback voltage, ΔL . $d_{33, \delta L}$ is deduced from δL and $d_{33, \Delta L}$ is obtained from the measurement of ΔL . At low frequencies $f_s < 0.1$ Hz, most of the slowly varying δL_D will be compensated by the feedback voltage, so that $d_{33, \delta L}$ reduces towards zero. At high frequency $f_s > 0.1$ Hz, the feedback loop cannot response fast enough and δL_D is mostly captured by δL . At sufficiently high frequencies $f_s > 1$ Hz, $d_{33, \Delta L}$ nearly vanishes so that $d_{33} = d_{33, \delta L} = 5.8$ pm/V, consistent with other reports²⁶⁻²⁹. In principle, one can extend the low frequency performance by changing the PID feedback param-

eters. However, it is not causing a problem in our α measurement, since the optimized frequency of our in-situ heating sample holder is about $0.1 \sim 2$ Hz.

IV. THERMAL EXPANSION MEASUREMENT

Finally, we demonstrate the performance of our dilatometer by studying the thermal expansion coefficient of BaFe_2As_2 , the parent compound of the "122" Fe-based superconductors. It is generally believed to have a first-order antiferromagnetic transition at T_N around 134K^{30,31}. We choose a sample with thickness $L = 210\mu\text{m}$ and weight $m = 5\text{mg}$. Fig. 4(a) shows the typically raw data of δT and δL using $f_S = 0.25\text{Hz}$ at $T_0 \simeq 130\text{K}$. The phases of these two oscillations are perfectly aligned so that the δL vs. δT plot in Fig. 4 (b) exhibit a linear relation whose slope is the α . This linear dependence evidences that the sample and sample holder are always at thermal equilibrium and have a uniform temperature, because a finite temperature gradient will result in a delay of the sample temperature and the measured thermal expansion δL from the temperature variation δT taken at the vicinity of the AC heater.

In our dilatometer, the sapphire sample holder is nearly thermally isolated from the rest of the system, so that its temperature change causes negligible thermal expansion of the structure. The black curve in Fig. 4(c) represents the measured $\langle \delta T \rangle$ when we sweep the DC temperature T_0 through the phase transition temperature T_N . From the measured $\langle \delta T \rangle$, we can calculate the total heat capacity C_{total} of the components that has been isolated together with the sample holder. According to the known heat capacity of BaFe_2As_2 ^{32,33}, sapphire and copper, we estimate that the heated structure includes the sapphire plate (15), sample (14) and the lower plate (16).

In addition, $\langle \delta T \rangle$ exhibits a dip at 133.7 K, signaling a maximum in C_{total} . This is consistent with the diverging specific heat of BaFe_2As_2 at its phase transition^{32,33}. We plot the measured sample's thickness change ΔL from the feedback voltage in Fig. 4(d). The 30-nm ΔL jump coincides with the C_{total} peak, as expected from the Ehrenfest and Maxwell relations.

Thanks to the extremely high resolution, our dilatometer reveals more features near the phase transition. Fig. 4(e) shows the AC thermal coefficient α measured using $\langle \delta T \rangle = 5$ mK, as well as sub-10 mK resolution in temperature. α exhibits a large negative peak near $T_N = 133.67$ K. The data measured with $t_c = 25$ s is plotted in black and the red curve shows the data measured with $t_c = 250$ s for better $\langle \delta L \rangle / L$ resolution. The overlapping of the two traces in Fig. 4(e) demonstrate the stability and accuracy of our dilatometer. Note that such high resolution in $\langle \delta L \rangle / L$ and the sub-10-mK resolution in temperature, is achieved simultaneously for a 210-micrometer-thickness sample!

V. CONCLUSION

In conclusion, we develop a contactless dilatometer based on optical Michelson interferometer. Our dilatometer is

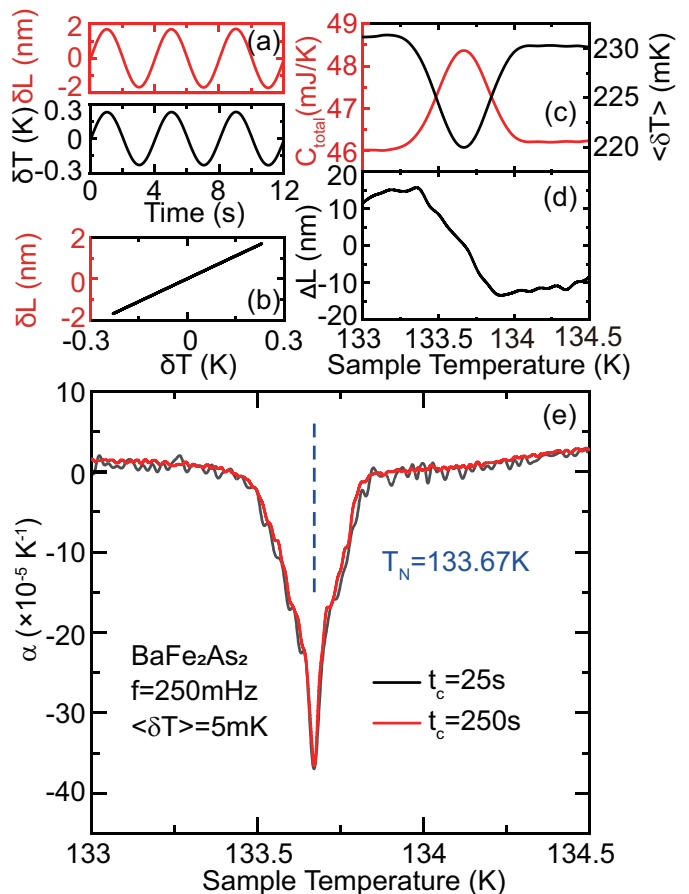


FIG. 4. α measured at $f_S = 0.25\text{Hz}$ from a BaFe_2As_2 sample with thickness $210\mu\text{m}$. (a) The δL and δT oscillation at $T_0 = 130$ K. (b) The linear relation between δL and δT of the data in (a). (c) The divergence of $\langle \delta T \rangle$ (black) when T_0 sweeps through the transition temperature. We can calculate the total heat capacity C_{total} (red) of heated components. (d) The ΔL measured synchronously with (c) data. (e) The AC α measured with $f_S = 0.25\text{Hz}$ and $\langle \delta T \rangle = 5$ mK using averaging time $t_c = 25$ and 250 s, respectively.

able to measure very thin and fragile samples with sub-pm-resolution in sample thickness change and mK-resolution in temperature, simultaneously. We demonstrate its performance by measuring the antiferromagnetism transition of BaFe_2As_2 . Besides the thermal expansion coefficient and piezoelectric coefficient measurement we demonstrate here, our setup can also be used for magnetostriction, magnetic torque and other measurements where a length change is introduced by a certain physics process. It's also possible to integrate multiple synchronous measurements and in-situ tuning in the future. Although it's difficult for us now to measure the absolute value of α because of residual AC background thermal expansion of a few nm/K level, both its extremely high resolution, accuracy and the contactless nature open a new playground for research in condensed matter physics. This prototype should be upgraded for better performance in the future.

ACKNOWLEDGMENTS

The work at PKU was supported by the National Key Research and Development Program of China (Grant No. 2021YFA1401900 and 2019YFA0308403), the Innovation Program for Quantum Science and Technology (Grant No. 2021ZD0302602), and the National Natural Science Foundation of China (Grant No. 92065104 and 12074010). The BaFe₂As₂ sample is supplied by Xingyu Wang, Huiqian Luo and Shiliang Li at the Institute of Physics, Chinese Academy of Sciences. We thank Mingquan He and Yuan Li for valuable discussion.

DATA AVAILABILITY STATEMENT

The data that support the findings of this study are available from the corresponding author upon reasonable request.

REFERENCES

- ¹G. K. White and M. L. Minges, *International Journal of Thermophysics* **18**, 1269 (1997).
- ²R. Modler, P. Gegenwart, M. Lang, M. Deppe, M. Weiden, T. Lühmann, C. Geibel, F. Steglich, C. Paulsen, J. L. Tholence, N. Sato, T. Komatsubara, Y. Ōnuki, M. Tachiki, and S. Takahashi, *Physical Review Letters* **76**, 1292 (1996).
- ³R. Lortz, C. Meingast, U. Welp, W. K. Kwok, and G. W. Crabtree, *Physical Review Letters* **90**, 237002 (2003).
- ⁴S. Zaum, K. Grube, R. Schäfer, E. D. Bauer, J. D. Thompson, and H. v. Löhneysen, *Physical Review Letters* **106**, 087003 (2011).
- ⁵A. E. Böhmer, P. Burger, F. Hardy, T. Wolf, P. Schweiss, R. Fromknecht, H. v. Löhneysen, C. Meingast, H. K. Mak, R. Lortz, S. Kasahara, T. Terashima, T. Shibauchi, and Y. Matsuda, *Physical Review B* **86**, 094521 (2012).
- ⁶F. Hardy, N. J. Hillier, C. Meingast, D. Colson, Y. Li, N. Barišić, G. Yu, X. Zhao, M. Greven, and J. S. Schilling, *Physical Review Letters* **105**, 167002 (2010).
- ⁷A. M. Nikitin, J. J. Geldhof, Y. K. Huang, D. Aoki, and A. de Visser, *Physical Review B* **95**, 115151 (2017).
- ⁸L. Rossi, A. Bobel, S. Wiedmann, R. Kuchler, Y. Motome, K. Penc, N. Shannon, H. Ueda, and B. Bryant, *Physical Review Letters* **123**, 027205 (2019).
- ⁹A. E. Petrova and S. M. Stishov, *Phys. Rev. B* **94**, 020410 (2016).
- ¹⁰J. L. Niedziela, L. D. Sanjeewa, A. A. Podlesnyak, L. DeBeer-Schmitt, S. J. Kuhn, C. de la Cruz, D. S. Parker, K. Page, and A. S. Sefat, *Physical Review B* **103**, 094431 (2021).
- ¹¹M. Jaime, C. Corvalán Moya, F. Weickert, V. Zapf, F. F. Balakirev, M. Wartenbe, P. F. S. Rosa, J. B. Betts, G. Rodriguez, S. A. Crooker, and R. Daou, *Sensors* **17**, 2572 (2017).
- ¹²A. Ikeda, T. Nomura, Y. H. Matsuda, S. Tani, Y. Kobayashi, H. Watanabe, and K. Sato, *Review of Scientific Instruments* **88**, 083906 (2017).
- ¹³L. Wang, G. M. Schmiedeshoff, D. E. Graf, J.-H. Park, T. P. Murphy, S. W. Tozer, E. Palm, J. L. Sarrao, and J. C. Cooley, *Measurement Science and Technology* **28**, 065006 (2017).
- ¹⁴Y. Gu, B. Liu, W. Hong, Z. Liu, W. Zhang, X. Ma, and S. Li, *Review of Scientific Instruments* **91**, 123901 (2020).
- ¹⁵R. Grössinger and H. Müller, *Review of Scientific Instruments* **52**, 1528 (1981).
- ¹⁶X. Ding, Y.-S. Chai, F. Balakirev, M. Jaime, H. T. Yi, S.-W. Cheong, Y. Sun, and V. Zapf, *Review of Scientific Instruments* **89**, 085109 (2018).
- ¹⁷G. O. J. B. F. Figgins and D. P. Riley, *The Philosophical Magazine: A Journal of Theoretical Experimental and Applied Physics* **1**, 747 (1956).
- ¹⁸M. Rotter, H. Müller, E. Gratz, M. Doerr, and M. Loewenhaupt, *Review of Scientific Instruments* **69**, 2742 (1998).
- ¹⁹R. S. Manna, B. Wolf, M. de Souza, and M. Lang, *Review of Scientific Instruments* **83**, 085111 (2012).
- ²⁰R. Kuchler, T. Bauer, M. Brando, and F. Steglich, *Review of Scientific Instruments* **83**, 095102 (2012).
- ²¹R. Kuchler, A. Wörl, P. Gegenwart, M. Berben, B. Bryant, and S. Wiedmann, *Review of Scientific Instruments* **88**, 083903 (2017).
- ²²R. Kuchler, R. Wawrzyńczak, H. Dawczak-Dębicki, J. Gooth, and S. Galeski, *Review of Scientific Instruments* **94**, 045108 (2023).
- ²³X. Qin, X. Wang, W. Hong, M. Geng, Y. Li, H. Luo, S. Li, and Y. Liu, “Electronic phase propagation speed in bafe₂as₂ revealed by dilatometry,” (2024), arXiv:2311.18442 [cond-mat.supr-con].
- ²⁴J.-F. Wang, X. Wang, H. Luo, and Z. Meng, *Acta Physica Sinica* **61**, 150701 (2012).
- ²⁵Y. Liu, L. Wang, C. Tian, M. Zhang, and Y. Liao, *Journal of Lightwave Technology* **26**, 3225 (2008).
- ²⁶W. Yue and J. Yi-jian, *Optical Materials* **23**, 403 (2003).
- ²⁷R. Smith and F. Welsh, *Journal of Applied Physics* **42**, 2219 – 2230 (1971).
- ²⁸H. Okamura and J. Minowa, *Electronics Letters* **25**, 395 (1989).
- ²⁹P. Zhang and W. Zhong, *ShanDong Science and Technology Press*, Page (s) **5**, 7 (1997).
- ³⁰M. G. Kim, R. M. Fernandes, A. Kreyssig, J. W. Kim, A. Thaler, S. L. Bud’Ko, P. C. Canfield, R. J. McQueeney, J. Schmalian, and A. I. Goldman, *Physical Review B* **83**, 134522 (2011).
- ³¹T. R. Forrest, P. N. Valdivia, C. R. Rotundu, E. Bourret-Courchesne, and R. J. Birgeneau, *Journal of Physics: Condensed Matter* **28**, 115702 (2016).
- ³²M. Rotter, M. Tegel, D. Johrendt, I. Schellenberg, W. Hermes, and R. Pöttgen, *Phys. Rev. B* **78**, 020503 (2008).
- ³³C. R. Rotundu, B. Freelon, T. R. Forrest, S. D. Wilson, P. N. Valdivia, G. Pinuellas, A. Kim, J.-W. Kim, Z. Islam, E. Bourret-Courchesne, N. E. Phillips, and R. J. Birgeneau, *Phys. Rev. B* **82**, 144525 (2010).